REPORT DOCUMENTATION PAGE

Form Approved
OMB No. 0704-0188

1. REPORT DATE *(DD-MM-YYYY)*	**2. REPORT TYPE**	**3. DATES COVERED** *(From - To)*
13-07-2009	Technical Paper	

4. TITLE AND SUBTITLE

Mixing Enhancement of Liquid Rocket Engine Injector Flow

5a. CONTRACT NUMBER

5b. GRANT NUMBER

5c. PROGRAM ELEMENT NUMBER

6. AUTHOR(S)
Juan Rodriguez (UCLA); Ivett Leyva, Jeffrey Graham, & Douglas Talley (AFRL/RZSA)

5d. PROJECT NUMBER

5f. WORK UNIT NUMBER
23080533

7. PERFORMING ORGANIZATION NAME(S) AND ADDRESS(ES)

Air Force Research Laboratory (AFMC)
AFRL/RZSA
10 E. Saturn Blvd.
Edwards AFB CA 93524-7680

8. PERFORMING ORGANIZATION REPORT NUMBER

AFRL-RZ-ED-TP-2009-273

9. SPONSORING / MONITORING AGENCY NAME(S) AND ADDRESS(ES)

Air Force Research Laboratory (AFMC)
AFRL/RZS
5 Pollux Drive
Edwards AFB CA 93524-7048

10. SPONSOR/MONITOR'S ACRONYM(S)

11. SPONSOR/MONITOR'S NUMBER(S)
AFRL-RZ-ED-TP-2009-273

12. DISTRIBUTION / AVAILABILITY STATEMENT

Approved for public release; distribution unlimited (PA #09319).

13. SUPPLEMENTARY NOTES
For presentation at the 45th AIAA Joint Propulsion Conference & Exhibit, Denver, CO, 2-5 August 2009.

14. ABSTRACT

An investigation of the mixing enhancement behavior of N2 shear coaxial jets between two injector geometries is presented. A total of 20 cases with one injector geometry and 15 with the other, corresponding to different momentum flux ratios (J's) at subcritical, nearcritical and supercritical pressures are analyzed and compared. The measurements are extracted from 998 backlit images. Acoustic excitation is used to analyze the response of the system to velocity and pressure perturbations. The frequency of the system varied from 2.90 to 3.11 kHz and the maximum peak-to-peak pressure perturbation as a percentage of the mean chamber pressure was 4%. It was found that changing the geometry of injectors of similar size had a large impact on the behavior of the coaxial jet. The qualitative response of one of the injectors to acoustics at low J's in the subcritical regime was completely different to the other. In contrast, when comparing cases with very similar J's, it was found that the normalized dark core length between these cases remains close regardless of phase angle for the two injectors despite the fact that the relative acoustic excitation intensities for subcritical pressures were up to eight times stronger than near and supercritical chamber pressures for one of the injectors and close to 2 times stronger for the other.

15. SUBJECT TERMS

16. SECURITY CLASSIFICATION OF:			**17. LIMITATION OF ABSTRACT**	**18. NUMBER OF PAGES**	**19a. NAME OF RESPONSIBLE PERSON**
					Dr. Douglas Talley
a. REPORT	**b. ABSTRACT**	**c. THIS PAGE**	SAR	21	**19b. TELEPHONE NUMBER** *(include area code)*
Unclassified	**Unclassified**	**Unclassified**			N/A

Mixing Enhancement of Liquid Rocket Engine Injector Flow

Juan I. Rodriguez[1]
Department of Mechanical and Aerospace Engineering, UCLA, Los Angeles, CA, 90095

Ivett A. Leyva[2], Jeffrey J. Graham[3] and Douglas Talley[4]
AFRL/RZSA, Edwards AFB, CA, 93524

An investigation of the mixing enhancement behavior of N_2 shear coaxial jets between two injector geometries is presented. A total of 20 cases with one injector geometry and 15 with the other, corresponding to different momentum flux ratios (J's) at subcritical, nearcritical and supercritical pressures are analyzed and compared. The measurements are extracted from 998 backlit images. Acoustic excitation is used to analyze the response of the system to velocity and pressure perturbations. The frequency of the system varied from 2.90 to 3.11 kHz and the maximum peak-to-peak pressure perturbation as a percentage of the mean chamber pressure was 4%. It was found that changing the geometry of injectors of similar size had a large impact on the behavior of the coaxial jet. The qualitative response of one of the injectors to acoustics at low J's in the subcritical regime was completely different to the other. In contrast, when comparing cases with very similar J's, it was found that the normalized dark core length between these cases remains close regardless of phase angle for the two injectors despite the fact that the relative acoustic excitation intensities for subcritical pressures were up to eight times stronger than near and supercritical chamber pressures for one of the injectors and close to 2 times stronger for the other.

I. Introduction

Mixing enhancement is one of many parameters that are important when considering Liquid Rocket Engine (LRE) performance. Thorough combination of the inner and outer jet streams in an LRE coaxial injector could lead to an increase of the total energy release from the propellants. To characterize mixing, several variables could be considered. However, for the purposes of this study, both the qualitative response of the coaxial jet and the length of the inner jet dark core length will be the chosen parameters to assess mixing between the inner and the outer jet in two different coaxial jet configurations. For instance, a shorter inner jet dark core means that mixing with its surroundings takes place faster than compared to a longer one at the same flow conditions. In previous studies, Gutmark et al.[1] concluded in their coaxial vs. free jet studies that in coaxial flow configurations more of the surrounding fluid is entrained deeper into the inner jet as compared to the free jet case, enhancing the overall mixing process. These researchers also found that the geometry of the injector plays a role as well, with better mixing performance achieved by rectangular injectors compared to circular ones. Gautam and Gupta[2] reported in their cryogenic coaxial injector studies at atmospheric pressures an increase in the evaporation of the inner jet and enhanced mixing with the surrounding flow with increasing outer to inner momentum flux ratio (J). They also change the geometry of their injector setup by modifying the recess length between the inner jet and the outer jet exits. They found that larger recess lengths promote higher jet expansion and more entrainment of surrounding gases into the flow. Their shear layer analysis confirms that mixing and jet expansion are slower at lower J's. Zong and Yang[3] also find in their numerical study of high pressure coaxial reactive flow that as the J increases, turbulent mixing is enhanced whereas the inner jet dark core is reduced. Finally, Richecoeur et al.[4] studied an acoustically excited, multiple element, and reactive coaxial injector configuration at elevated but still subcritical pressure conditions. They found that conditions where combustion became sensitive to external oscillations happened at lower J's. The strong coupling between acoustics and combustion showed an enhancement of the flame spread at a

[1]Research Associate, UCLA, Los Angeles, CA 90095-1597, AIAA Member.
[2]Lead, Combustion Dev. Group, AFRL/RZSA, 10 E. Saturn Blvd., Edwards AFB, CA 93524, AIAA Sr. Member.
[3]Combustion Scientist, 1st Lt., AFRL, Edwards AFB, CA 93524, AIAA Member.
[4]Sr. Aerospace Engineer, AFRL/RZSA, 10 E. Saturn Blvd., Edwards AFB, CA 93524, AIAA Member.

pressure antinode location, where pressure perturbations are the highest, which might be associated with improved mixing.

Therefore, the overall objective of our study is to provide an analysis of mixing enhancement in a coaxial injector flow, which is a type of injector extensively used in LRE's. Two different coaxial injector geometries will be studied and in addition to varying J and the chamber pressure, acoustic forcing is used to generate different velocity and pressure perturbation conditions at the location of the jet. These transversal pressure and velocity fields are generated with two piezo-siren elements that produce high amplitude acoustics. The phase between them can be adjusted so the position of the jet with respect to the generated pressure and velocity fields can be varied. The resonant frequency is around 3 kHz and pressure perturbations can reach values as high as 4% of the chamber pressure. The experimental study is conducted at three different pressure regimes ranging from 1.5 to 5.0 MPa, spanning subcritical to supercritical pressures, with J varying from 0.019 to 23. By maintaining similar outer to inner jet momentum flux ratios between the two geometries, conclusions will be drawn on the effect of having a relatively thick versus a thin wall between the inner and outer jet flows in a coaxial jet configuration. Very recent results from our research group show that a thicker post could create a recirculation zone that prevents or at least delays unstable behavior of the inner jet in certain flow regimes[5,6].

II. Experimental setup

The experimental work presented in this study was performed at the Air Force Research Laboratory, Edwards Air Force Base, CA. The Cryogenic Supercritical Laboratory (EC 4) was used to run all tests. A photograph of the facility is shown in Fig. 1.a and a schematic of the experiment is shown in Fig. 1.b. The photograph shows the test chamber in the center and the acoustic drivers on each side. The chamber flow exits through a vent line located at the center bottom of the chamber. Above the chamber there is a thick insulation that houses the inner jet heat exchanger which cools the nitrogen inner jet as much as possible before it enters the chamber. On top of the chamber, to the sides of the insulation, there are orifices that allow more probes, such as thermocouples and pressure transducers, to reach inside the test chamber. On the back, towards the right side of the photograph, part of the control panel can be observed, where valves, flow meters and pressure regulators were used to monitor and distribute the right amount of flow to the experimental setup.

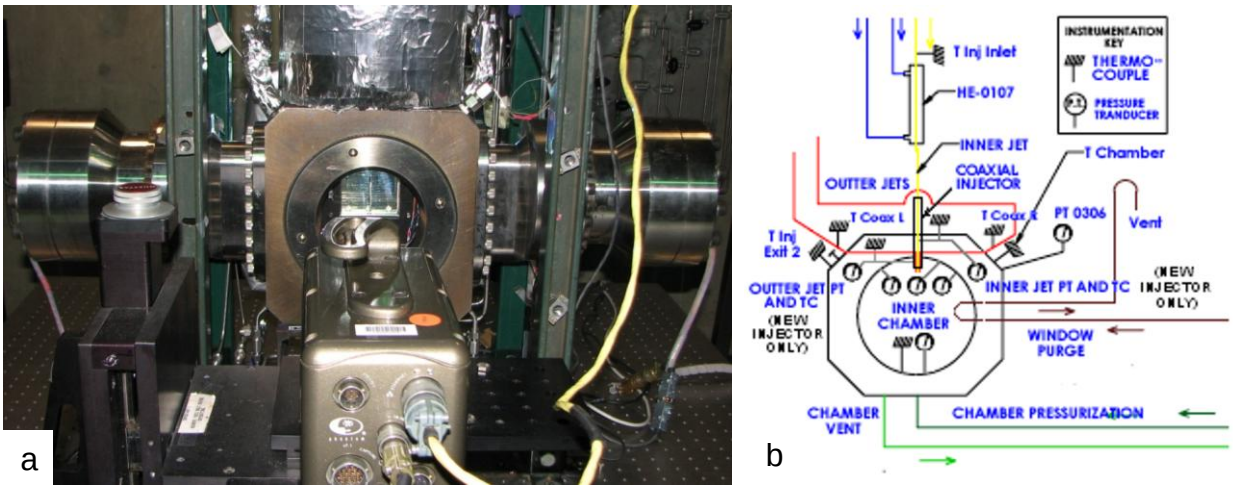

Figure 1a. Experimental test chamber and supporting systems of the Experimental Cell 4 at AFRL, Edwards AFB, CA. b. Chamber section view of the flow schematic for Experimental Cell 4.

The chamber section of the schematic in Fig. 1.b represents the most updated version of the experimental setup. It shows the three differential pressure transducers that were used to measure the pressure fluctuations in three equally spaced locations with one placed just above the location of the coaxial injector exit and the other two to its sides. It also shows the pressure transducer and thermocouple that were brought from the bottom of the chamber to the injector exit inside the inner chamber. The schematic also shows that both the inner jet and outer jet have a pressure transducer and a thermocouple at the coaxial injector location. Also shown in the schematic in Fig. 1.b are heat exchangers that allowed the cooling of the inner and outer flows, and the window purge flow that was used to prevent water vapor condensation on the test chamber windows so as to allow proper visualization of the coaxial jet

flow. Several thermocouples were used across the heat exchanger and in other locations to keep track of the conditions of the flow in order to maintain the required flow properties for each test. To run one of these tests, gaseous N_2 was used to supply the inner and outer flows of the coaxial jet and to pressurize the chamber. Then the outer jet was cooled by either one or two heat exchangers (HEs), depending on the test requirements. A third HE was used to decrease the temperature of the inner jet. The coolant that ran through the HEs for both the inner and outer jets consisted of liquid N_2 obtained from a cryogenic pressure vessel located outside EC 4, which had a capacity of 5 m^3. The temperatures of the two jets were controlled by adjusting the flow rate of liquid N_2 through the HE's. The mass flow rates through the inner and outer jets were measured before they were cooled with Porter mass flow meters (models 122 and 123-DKASVDAA), since it was less cumbersome to measure mass flow rates at ambient temperature than to measure them at cryogenic conditions.

Once the desired mass flow rates for the inner and outer jet were achieved, the mean chamber pressure required for the experiment was adjusted. The chamber pressure was measured with a Stellar 1500 transducer. After the mean chamber pressure was obtained, the mass flow rates were adjusted for minor changes due to the pressure increase. Finally, the liquid N2 flow through the HEs was carefully controlled to stabilize the inner and outer jet temperatures to produce the desired outer to inner jet momentum flux ratio for that particular test. To see a summary of the operating conditions achieved for all cases reported in this study, refer to the Appendix. In order to maximize the effect of the available acoustic energy on the jet, an inner chamber was created into which the jet is injected. This inner chamber had a nominal height of 6.6 cm, a width of 7.6 cm and a depth of 1.3 cm. At the bottom of the inner chamber an aluminum piece served as support and on the top there was a plate that acted as the 'ceiling'. Both the top and bottom pieces had orifices at their centers. The top plate's orifice allowed the coaxial jet tip to enter the inner chamber and the bottom orifice was used to provide an exit for the flow. It was also used to introduce a thermocouple and pressure transducer to study the properties of the flow near the jet.

Two images of the first or "original" coaxial injector used in these studies are shown in Figs. 2.a and b. Fig. 2.a presents the full injector and Fig. 2.b shows a plane view of the end where the jets exited. The inner diameter of the inner jet, D_1, or $2R_1$ as shown in the picture, was 0.51 mm. The outer jet had an inner diameter, D_2, of 1.59 mm and outer diameter, D_3, of 2.42 mm. The outer diameter of the injector, D_4, was 3.18 mm. The length to inner diameter ratio was 100 for the inner jet and 67 for the outer jet (taking as reference one half of the hydraulic diameter, $R_3 - R_2$). The coaxial injector was installed so that the inner and outer jets were concentric and the inner jet exit plane was recessed by 0.3 mm from the outer jet exit plane. This recess length was chosen to represent one half of D_1 in order to mimic realistic coaxial jet configurations used in industry.

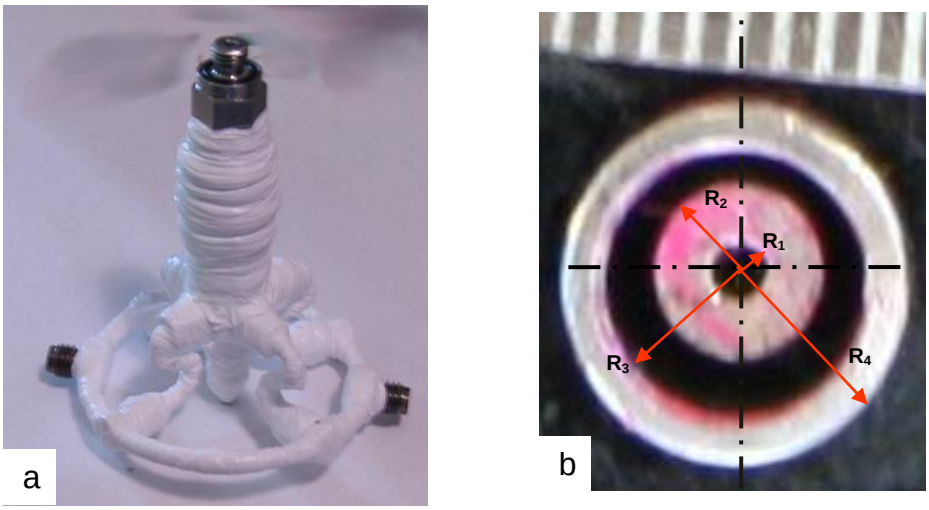

Figure 2.a. First ("original") coaxial injector used in this study. b. Exit plane view of the original coaxial injector.

The second or "new" coaxial injector used in these studies is shown in Figs. 3.a and b. The inner diameter of the inner jet, D_{new1}, or $2R_{new1}$, was 1.40 mm. The outer jet had an inner diameter, D_{new2}, of 1.65 mm and outer diameter, D_{new3}, of 2.44 mm. The outer diameter of the injector, D_{new4}, was 3.94 mm. The length to inside diameter ratio was 65 for the inner jet and 105 for the outer jet (taking as reference one half of the hydraulic diameter, R_{new3} –

R_{new2}). The injector was installed so that the inner and outer jets were concentric and the inner jet exit plane was recessed by 0.7 mm from the outer jet exit plane, which was chosen to represent one half of D_{new1}, to be able to compare it with the results obtained with the original injector. Note that the inner post thickness decreased dramatically from the original injector to the new injector. The post thickness of the original injector was 110% of its inner diameter ($1.1D_1$) whereas the post thickness of the new injector is only 9.1% of its inner diameter ($0.091D_{new1}$).

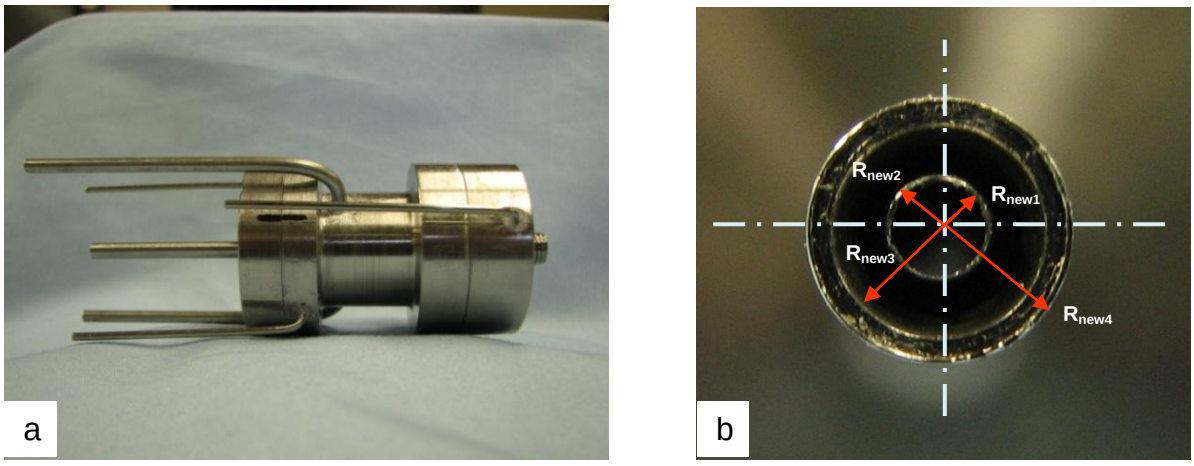

Figure 3.a. Second ("new") coaxial injector used in this study. b. Exit plane view of the new coaxial injector.

The temperature of the fluid in the jets was measured with unshielded type E thermocouples with a bead diameter of 0.1 mm. The accuracy of the thermocouples used in the study was checked with an RTD and found to be within ±1 K. A miniature pressure transducer was placed next to the thermocouple, using a small metallic post as support, and used to measure the pressure at a sampling frequency of 20 kHz. The manufacturer of the miniature pressure transducers was Kulite Semiconductor Products, Inc. (models CCQ-062-1000A and CCQ-093-750A). These pressure transducers had an absolute pressure range of either 6.9 MPa or 5.2 MPa, respectively. The thermocouple and pressure transducer probe used are shown in Fig. 4. In this photograph, the upper boundary or 'ceiling' of the inner chamber and the tip of the injector discussed above can be clearly seen.

Figure 4. Thermocouple and pressure transducer probes near the exit of the coaxial injector.

Two linear positioning stages built by Attocube Systems AG were used to move the pressure transducer and the thermocouple in a plane perpendicular to the jet axis. Each stage had a range of 3 mm in 1 dimension with step sizes in the order of 0.01 mm. One stage was placed on top of the other with their axis of movement perpendicular to each other for a total maximum examination area of 3 mm by 3 mm. With the configuration described above, the thermocouple tip could easily reach the exit plane of both the outer jet and inner jet. It was even possible to measure the temperature within the recess of the inner jet. The thermocouple and pressure transducer were attached to a custom made probe stand which in turn was affixed to the top of the linear positioning assembly using a small custom made base placed at the top end of a shaft that rested on a large, linear mechanical stage. The 10-cm range stage built by SETCO allowed the probe to get to the desired interrogation region within the inner chamber.

Properties such as density and viscosity were computed from the measured flow rates, chamber pressure and jet temperature, using the National Institute of Standards and Technology's REFPROP Software and its thermophysical properties online database[7,8]. From these properties, Reynolds number, Re, outer to inner jet velocity ratio, VR, and outer to inner jet momentum flux ratio, J, for a given set of conditions were then calculated. The jet was visualized by taking backlit images using a Phantom v7.1 high-speed camera capable of recording up to 160,000 frames per second at a resolution of 32 pixels by 32 pixels. For a resolution of 128 pixels by 256 pixels the camera was capable of recording 41,300 pictures per second. The resolution of the images in the present experiments varied from 128 pixels x 224 pixels to 196 pixels x 400 pixels, depending on chamber pressure and outer to inner momentum flux ratio. These in turn determined the size of the visible features of the jet that this study was characterizing. Each pixel represents an approximate area of 0.08 mm x 0.08 mm. Depending on the resolution chosen, the framing rate (frequency at which pictures were recorded) was 20, 25 or 41 kHz.

To focus the camera on the coaxial jet flow an AF Nikkor 35-105 mm lens, a Nikon No. 1 Close-Up lens, and various optical extensions were used. Since focusing on the outer jet structures while at the same time having a clear view of the inner jet was always a difficult process when setting up the camera and related optical equipment, the quality of the coaxial jet images was not always the same. The jet was backlit using a Newport variable power arc lamp set at 160 W or 300W. The exposure time generally was 1-2 μs and the number of images saved per run was 1000 on average. The dark core length and the inner jet spreading angles were measured from 998 images using a MATLAB subroutine based on the Otsu technique[9], which analyzes an image and finds a threshold which helps differentiate the dark core of the inner jet from the rest of the image.

The acoustic waves were generated using two piezo-sirens placed at each end of the chamber, custom-designed for the Air Force Research Laboratory by Hersh Acoustical Engineering, Inc. A Fluke 100 MS/s arbitrary waveform generator (model 292) was used to produce two sinusoidal waves with the same frequency but with a prescribed phase between them. The signals were then sent to two amplifiers, one for each piezo-siren. The amplifiers were a Krohn-Hite (model 7500) and a Trek (model PZD2000A), which amplified the signals and fed them to the piezo-sirens. The amplified signals were in the 200 to 540 V range. The principle by which the piezo-sirens work as acoustic drivers is relatively simple, with a piezo element moving an aluminum cone attached to it, which in turn vibrates to produce acoustic waves. The distance from each cone to the location of the coaxial jet is 44 cm. The frequency at which the piezo-sirens were driven was chosen by manually varying the frequency on the signal generator until the highest amplitudes of the pressure perturbations were obtained. These pressure perturbations were measured using the three differential Kulite pressure transducers (model XCQ-093-25D) flushed with the acrylic window of the inner chamber and recorded for further processing using Pacific Instruments PI660 Acquisition and Control Software.

The phase difference, also referred to in this work as phase angle, between the signals sent to the piezo-siren elements was varied to expose the coaxial jet to different effective positions relative to the pressure node or antinode of the generated acoustic field. When the two piezo-siren elements produce waves with a zero degree phase angle between them, the movement of the piezo-siren cones is synchronized and in opposite directions, that is, towards and away from each other. This produces conditions of high pressure perturbations and low velocity fluctuations at the center of the chamber, where the coaxial jet is located. This condition is called a pressure antinode or velocity node. In contrast, when the two drivers present a 180-degree phase difference, then the cones move in the same direction, generating high velocity fluctuations with very small variations in pressure at the jet location. This condition is called a pressure node or velocity antinode. A schematic of this behavior is reproduced in Fig 5.

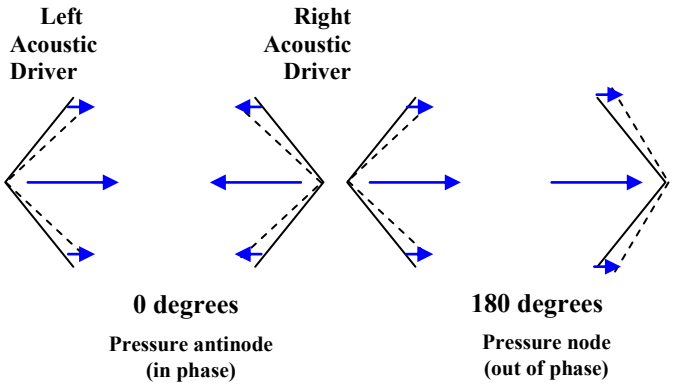

Figure 5. Simplified diagram of the two acoustic drivers at a 0° and 180° phase angle, indicating relative flow perturbation directions.

In these experiments, the voltage supplied to the two acoustic drivers was maintained at the same level for all conditions during each case. Efforts were made to keep the amplitudes of both piezo-siren elements the same. The piezo-sirens can be seen at both sides of the chamber in the photograph shown in Fig. 1.a. Since the experimental setup uses a rectangular test section, the jet was excited with a transverse acoustic field. A transverse mode on a rectangular chamber would be the equivalent of a tangential mode on a cylindrical chamber, which are the most dangerous for the integrity of such systems and an important reason to analyze its effects on a coaxial jet. To accommodate for the rectangular chamber, a waveguide with a catenary contour was used to transmit the waves from a circular cross-section to a rectangular cross-section. The maximum root-mean-square acoustic pressure fluctuations generated by the two piezo-ceramic acoustic sources in the inner chamber varied from 8.0 to 22 kPa and were produced in the 2.9 to 3.1 kHz range.

III. Results

To assess the effects of geometry on the behavior of the jet and mixing, the results of the original injector were compared to those with the new injector. The next sets of images show the response of the coaxial jet with the original and new injector at similar pressures and J values with the same levels of acoustic excitation. To obtain similar outer to inner momentum flux ratios with the new injector than those obtained with the original injector, the mass flow rate of the inner jet had to be increased by a factor of three. This change in mass flow rate was necessary given the difference in the inner jet inner diameter between D_1 and D_{1new} (see Figs. 2 and 3) between the original and new injectors. The first set of images is shown in Fig. 6.a. It corresponds to the case where J = 0.17 with the original injector. At this low momentum flux ratio at subcritical pressures the jet is usually thin. The overall behavior of the jet does not change substantially with and without acoustic forcing but an increase in mixing can be observed. For the 0° and 315° conditions the inner jet starts spreading and breaking up into smaller dark core sections that mix with the outer jet towards the middle of the image. In contrast, the 135° and the baseline conditions show very little spread and the core only starts to break up towards the bottom of the image.

The images shown in Fig. 6.b correspond to a momentum flux ratio of approximately 0.089 with the new injector. The first image on the top left shows the coaxial jet when no acoustics are present. The inner jet can be clearly distinguished from the outer jet and its surroundings. The thickness of the inner jet stays constant throughout the image and it is longer than the available field of view with a non-dimensional dark core length of at least 14 L/D_{1new} and most likely significantly longer based on the results from the original injector at similar momentum flux ratios. For the phase angles from 0° to 90 ° the inner jet bends noticeably too and there is strong atomization taking place near the injector exit. The background flow of the chamber is difficult to notice and the dark core region is somewhat thicker and blurred. The next two images show a perturbed, but straight, inner jet. The images corresponding to a phase difference between 225° and 315° show the liquid stream from the inner jet shortened significantly, with large structures of liquid that have been separated from the inner jet flowing downstream. The last image seems to return to the behavior seen at a 0° phase angle.

It is interesting to notice that the images that show the greatest contrast in the inner jet behavior with acoustics correspond to a phase difference of 135° and 315°, which would correspond to the pressure node and pressure antinode locations. In all phase angle conditions, the effect of the acoustic field on the integrity of the inner jet is something that was not observed with the original injector before, especially at these low momentum flux ratios. A possible cause of this phenomenon is the change in geometry from the original injector to the new injector. As discussed previously, the original injector featured a very thick inner jet post which created a large recirculation zone between the inner jet and the outer jet at the exit of the injector. This recirculation zone could have damped the pressure and velocity fluctuations, which instead of affecting the inner jet directly, modified the dynamics of the recirculation zone[10] which in turn altered the dynamics of the inner jet at the exit. That would explain the smooth back-and-forth oscillations of the inner jet that were characteristic of "strong evidence of acoustic excitation" with the original injector. However, without such a large recirculation zone, the pressure and velocity fluctuations could be having a direct impact on the inner jet flow and that might explain the very strong atomization taking place right at the exit of the injector for every acoustic condition regardless of phase angle.

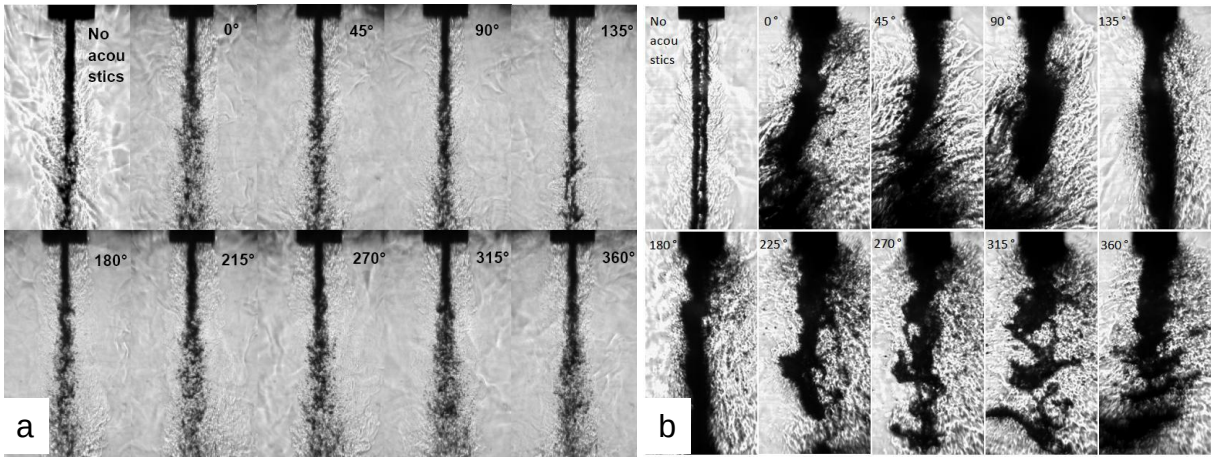

Figure 6.a. Collection of subcritical coaxial jet images at $P_{chamber}$ = 1.50 MPa, J = 0.17 with original injector geometry. b. Images with $P_{chamber}$ = 1.48 MPa, J = 0.089 with new injector geometry.

The second set of subcritical images corresponds to a momentum flux ratio between 2 and 3. The effects of the acoustics in this set of images with the original injector, shown in Fig. 7.a, are very clear. The inner jet dark core bends significantly for every phase angle reaching a maximum at 180°. Mixing improves significantly with large regions where the dark core structures have almost completely blended with their surroundings. This effect is particularly enhanced for phase angles between 45° and 215°. For the rest of the conditions a few dark fluid structures can still be observed throughout the image, but for the phase angle range mentioned the images show very few dark structures beyond certain point near the center. This sequence of images shows that the effects of high velocity fluctuations (pressure node conditions) due to acoustic forcing are very strong and can make a difference in practical systems operating near this momentum flux ratio. The set of images in Fig. 7.b show the coaxial jet behavior at a subcritical pressure of 1.49 MPa and momentum flux ratio of 2.0 for the new injector. The baseline condition shows a wide dark core region that does not extend the whole length of the image, in contrast with the previous two cases. In the first few inner jet diameters after the exit of the injector the dark core region is thick and connected, then it starts being sheared apart by the outer jet and becomes thinner with shreds of flow extending from the core towards the end. At the bottom of the image only a very thin dark core region, which is most likely unconnected from the main core, remains. The only noticeable difference is that the images at 135° and 180° do not show an hourglass shape but instead they seem to show similar dynamics to the baseline condition and even a longer dark core region. The original and new injector show that the effect of acoustics at this J value is siginificant but its particular manifestation can vary significantly with coaxial jet geometry.

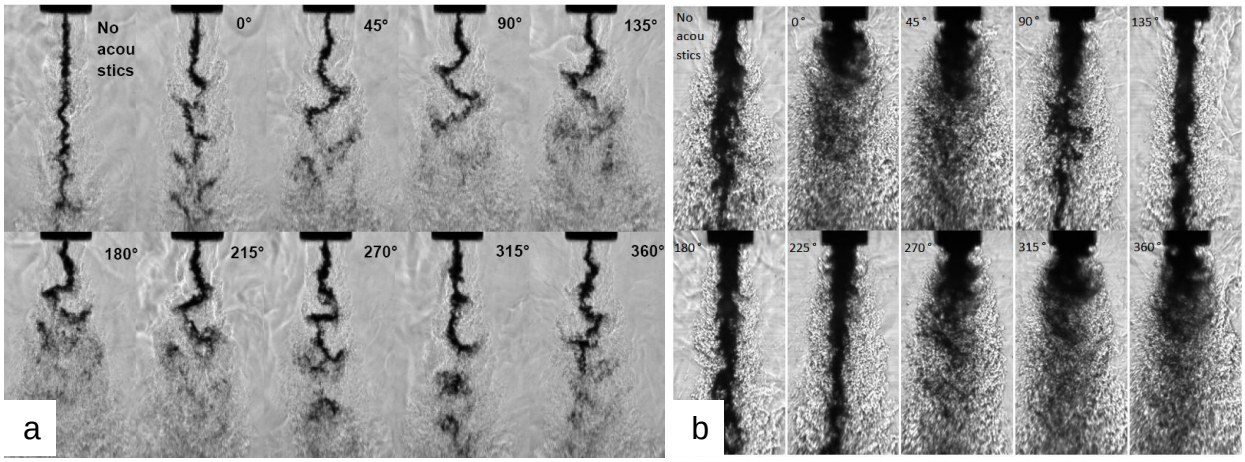

Figure 7.a. Collection of subcritical coaxial jet images at $P_{chamber}$ = 1.45 MPa, J = 2.6 with original injector geometry. b. Images at $P_{chamber}$ = 1.49 MPa, J = 2.0 with new injector geometry.

The next set of images for the subcritical case with the original injector is shown in Fig. 8.a and corresponds to a momentum flux ratio of 9.6. All the images feature a very thick dark core which differs substantially from the thin dark core regions observed in the previous two sets of images with the original injector. This thickness is evidence that the high momentum flux of the outer jet is having a strong effect on the inner jet allowing it to expand very rapidly across the recirculation region at the exit of the injector. The recess length of the inner jet hides this phenomenon and we only observe a thick jet emanating from the exit. Even at this high momentum flux ratio the dark core region is affected by the acoustic forcing as seen by the curvature of the inner jet for all phase angles, an effect that might not be obvious if only the effects of the dark core length are considered. For the original injector, the acoustics have a "bending" effect on the dark core. In contrast, the images in Fig. 8.b, which feature a momentum flux ratio of 7.8 with the new injector, are affected by the acoustic field in a completely different manner. It seems to induce a periodic "pulsation" of the inner jet. The behavior with acoustics is similar to the "expanding" case for J = 2.0 in Fig. 7.b, although the structures are clearer for this case. Again, with the new injector at 0° and 360° phase angle the structures are periodic, extend outward and wrap around forming eddies and near 180° phase angle the image is very similar to the case with no acoustics.

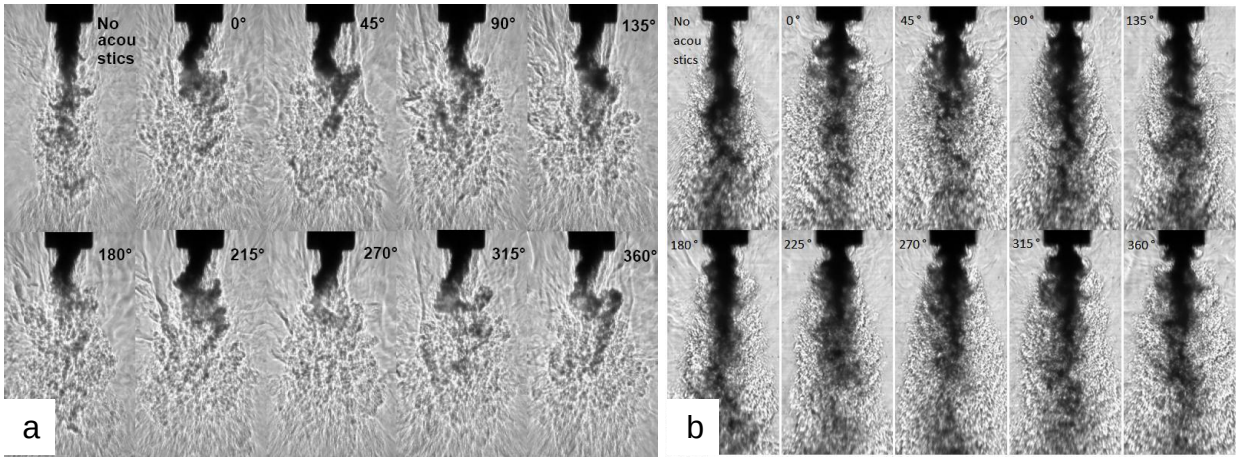

Figure 8.a. Collection of subcritical coaxial jet images at $P_{chamber}$ = 1.50 MPa, J = 9.6 with original injector geometry. b. Images at $P_{chamber}$ = 1.49 MPa, J = 7.8 with the new injector geometry.

The last set of images for a subcritical case with the orignal injector corresponds to a momentum flux ratio of 23. Fig. 9.a shows a dark core that does not seem to vary at all among the images and the only difference is the slight change in curvature at towards the bottom of the dark core for different acoustic conditions. The new injector equivalent is shown in Fig. 9.b. In this case the effect of the acoustics are still visible with a very short dark core at a 0° and 360° phase angle and longer dark cores near the 180° phase angle. For the new injector, acoustic effects are noticed in the dynamics of the dark core at subcritical pressures for momentum flux ratios near 20, since the dark core is still long enough to interact with the acoustic field, unlike the original injector where the effects of acoustics could not be adequately quantified by measuring the short dark core region from the images at these high J values.

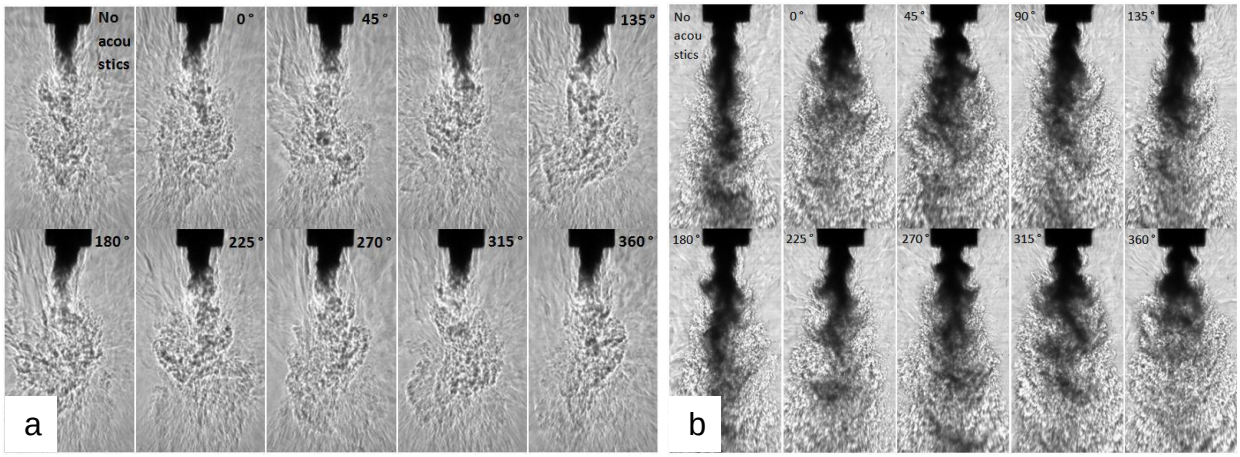

Figure 9.a. Collection of subcritical coaxial jet images at $P_{chamber}$ = 1.50 MPa, J = 23 with original injector geometry. b. Images at $P_{chamber}$ = 1.48 MPa, J = 18 with the new injector geometry.

The next figure shows a nearcritical case where the momentum flux ratio is near 10. The case with the original injector is shown in Fig. 10.a. In this set of images, the dark core is extremely short, and the effects of the acoustics, if any, are not discernible. On the other hand, Fig. 10.b shows a dark core which is effectivle reduced by imposing an acoustic field. The longest dark core is seen at the conditions with no acoustics followed by the condition at 180°. As the phase difference approaches 0° or 360° the effects of acoustics are more evident, with a shortening of the dark core and periodic structures emanating from the exit of the injector.

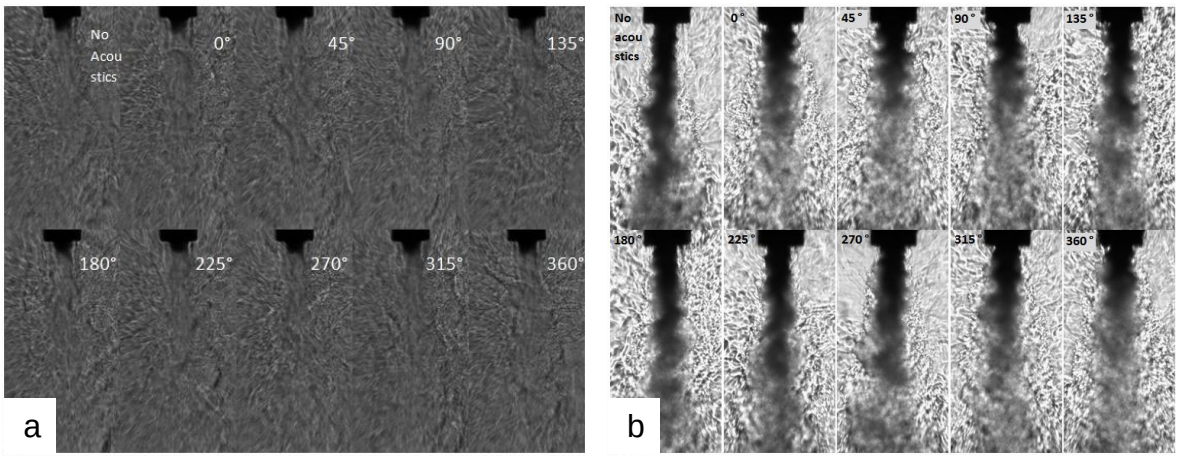

Figure 10.a. Collection of nearcritical coaxial jet images at $P_{chamber}$ = 3.56 MPa, J = 9.3 with original injector geometry. b. Images at $P_{chamber}$ = 3.58 MPa, J = 9.4 with the new injector geometry.

A comparison of two supercritical cases is presented in Fig. 11. The momentum flux ratio is approximately 2.5. The first set of images in Fig. 11.a represent the case with the original injector. The dark core lengths with acoustics are all shorter than the no acoustics condition. Another effect of the acoustics is the slight bending of the inner jet dark core. In contrast, the supercritical case with the new injector in Fig. 11.b features a very long dark core, which was not captured in its entirety by the camera. Acoustics did not seem to have any effect on it and all conditions show very similar images. It is difficult to make a conclusion for the case with the new injector since the complete length of the dark core is not visible.

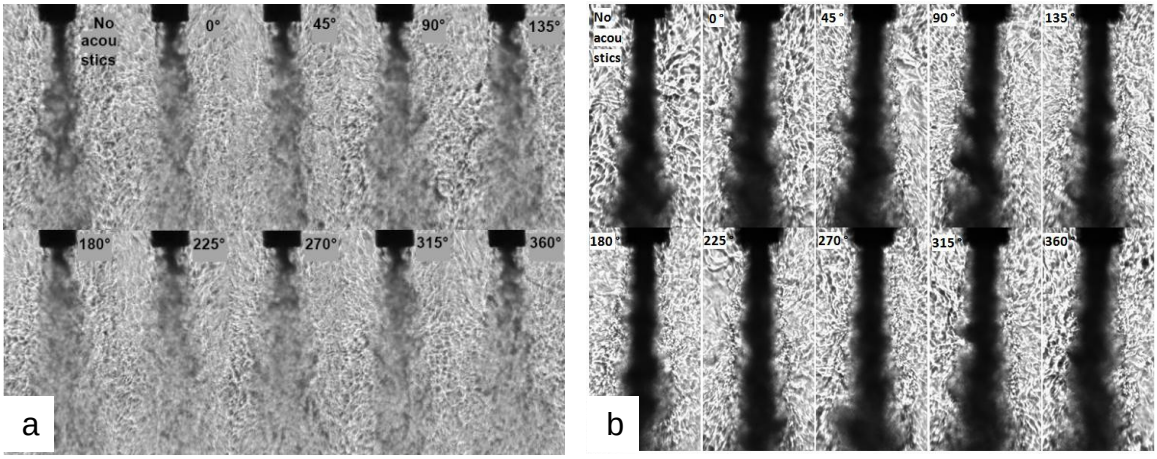

Figure 11.a. Collection of supercritical coaxial jet images at $P_{chamber}$ = 4.96 MPa, J = 2.4 with original injector geometry. b. Images at $P_{chamber}$ = 4.95 MPa, J = 2.6 with the new injector geometry.

The results of the dark core length measurements of the inner jet of the coaxial jet with the original and new injector flow are presented next. The following figures show a series of plots with the dark core length measurements on the vertical axis and the different acoustic conditions on the horizontal axis. A secondary axis shows the amplitude of the pressure oscillations as a fraction of the recorded mean chamber pressure for that case. The first value on the horizontal axis is the baseline measurement without acoustics followed by the measurements of the dark core length with acoustics starting with a 0° phase angle between acoustic sources and then in steps of 45° until a full cycle is achieved at 360°. All the values are normalized by the baseline condition of the case, which is the length of the dark core without acoustics. The error bars show the composite uncertainty of the non-dimensional length variable, $L_{acoustics}/L_{no\ acoustics}$, using one standard deviation as the uncertainty of each measured variable. As a reminder, the tests at subcritical pressures represent a two-phase coaxial jet flow, where the inner jet is in liquid state at a temperature below the critical temperature of N_2, and the outer jet is in a gaseous state at a temperature above the critical temperature of N_2.

The subcritical tests with the original injector in Fig. 12 showed that for J = 0.17, the largest dark core coincided with the condition of lowest pressure perturbations. The dark core length results for J = 1.0 do not show any trend, in contrast with the corresponding acoustic measurements which show a wave-like pattern. For J = 2.6, the lowest pressure oscillations occur at the same conditions as the largest changes in length. For J = 4.2, the largest length values occur near but not at the conditions where acoustic forcing is the lowest. For J = 9.6 and 23, the outer jet has even more momentum flux compared to the inner jet, making the dark core very short and irresponsive to the acoustics. For these cases, a clear trend linking the longest dark cores and a particular condition in the acoustic field could not be identified.

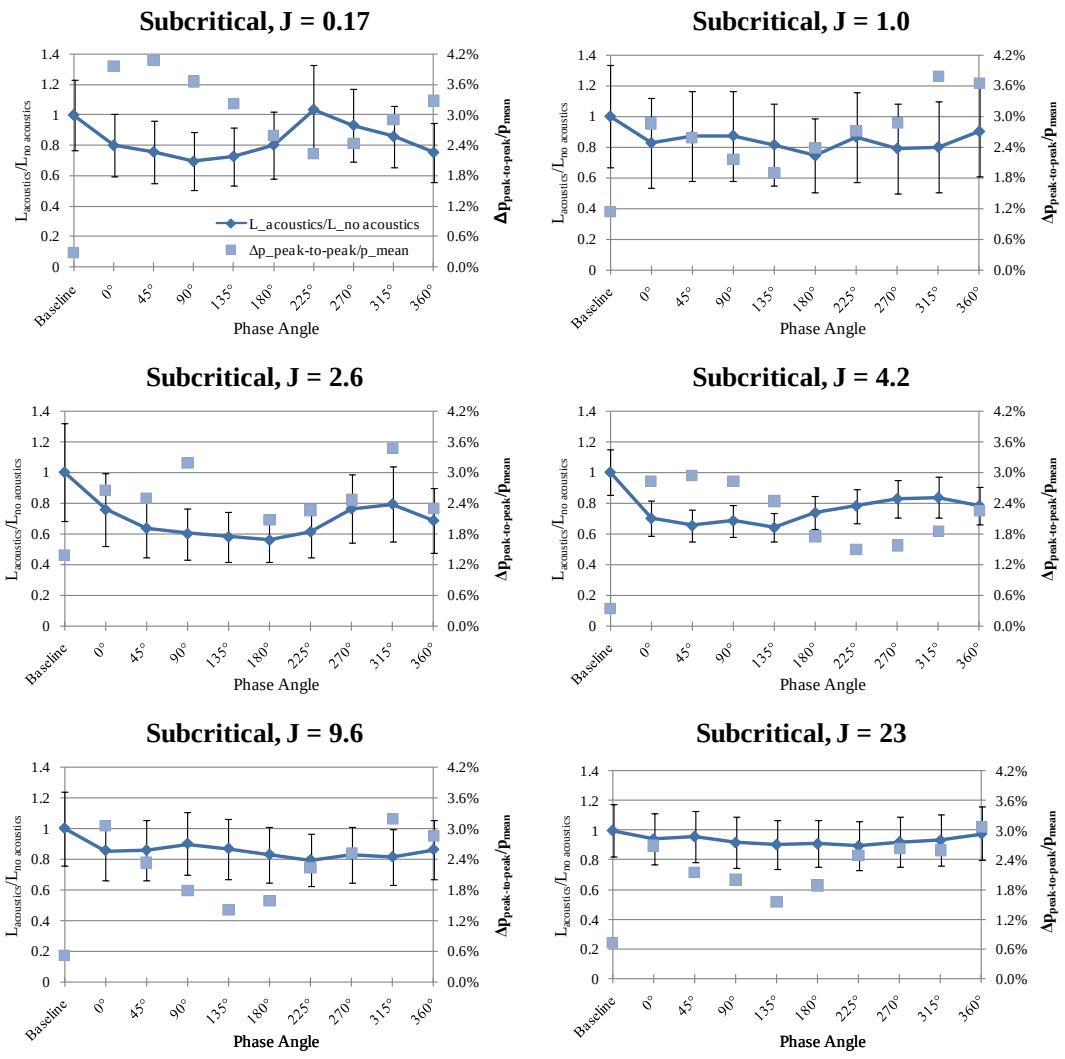

Figure 12. Dark core length with acoustics ($L_{acoustics}$) over dark core length without acoustics ($L_{no\ acoustics}$), shown in diamonds, versus phase angle between acoustic sources for subcritical pressures. The the peak-to-peak pressure perturbation as a percentage of the mean chamber pressure ($\Delta p_{peak\text{-}to\text{-}peak}/p_{mean}$), in squares, is also plotted. Original injector geometry.

The values of the dark core lengths with the new injector for the tests at subcritical pressures are shown in Fig. 13. As the J value of the case decreased, at some or all conditions as explained in the caption of the figure, the dark core length was longer than the image obtained from the camera. Thus, accurate dark core measurements could not be obtained for those conditions. However, a semi-quantitative analysis can still be made for some of those cases. For instance, the cases with J = 0.43 and 2.0 had dark core lengths that were measurable for half of the phase angles. The conditions for which the dark core was too long were those near the pressure node as indicated by the pressure data shown in the plots. The conclusion can be made that for these cases the longest dark core lengths were close to the condition with the lowest pressure perturbations. For the next two plots in Fig. 13, for J equal to 3.4 and 5.2, the same trend with phase angle can be observed. The last three plots in Fig. 13 show the reduction in the dark core length for J = 7.8, 12 and 18. These plots show longer dark core lengths at the location of the pressure node.

The general trend observed in these measurements consists of longer dark cores near the pressure node and very short ones near the pressure antinode. One of the possible explanations for this effect might involve the lack of recirculation zone in the new injector. The recirculation zone could be responsible for the bending of the jet at high velocity fluctuations but in the case of the new injector this recirculation zone is non-existent and the bending does not take place, thus a straight dark core is observed.

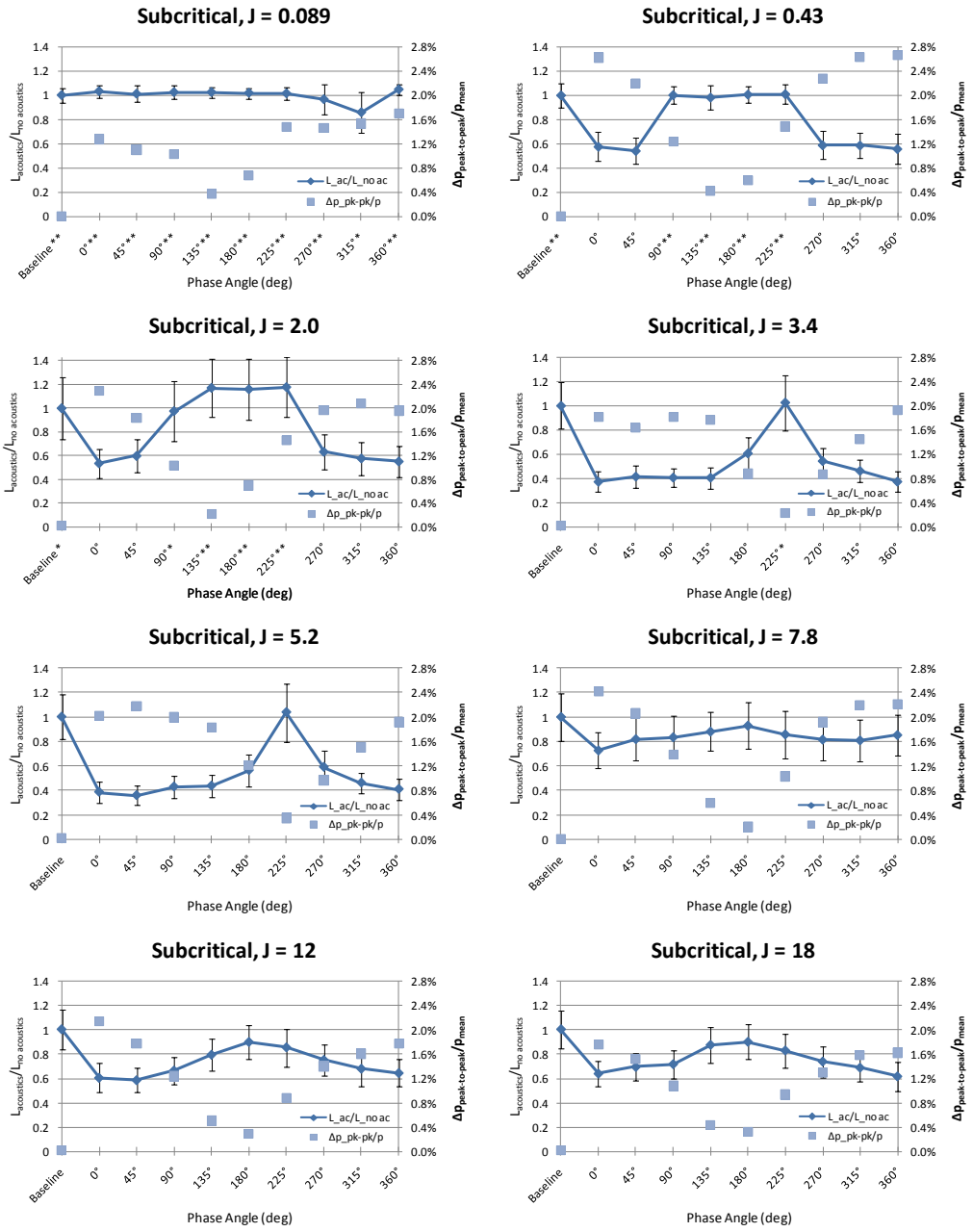

Figure 13. Dark core length with acoustics ($L_{acoustics}$) over dark core length without acoustics ($L_{no\ acoustics}$), shown in diamonds, versus phase angle between acoustic sources for subrcritical pressures. The the peak-to-peak pressure perturbation as a percentage of the mean chamber pressure ($\Delta p_{peak\text{-}to\text{-}peak}/p_{mean}$), in squares, is also plotted. The cases which had their x coordinate marked with an asterisk (*) denote cases that had a dark core length that was longer than the field of view in more than 10% but less than 50% of the images. The ones marked with two asterisks (**) had dark cores larger than the examination window for at least half of the images. New injector geometry.

The next set of graphs shown in Figs. 14 and 15 show the results for the tests performed at nearcritical and supercritical pressures with the original injector. At these pressures, the coaxial jet flow had only one supercritical phase present since both the temperature and pressure of the inner and outer jet, as well as the surrounding environment, was above the critical temperature and pressure of N_2.

For most nearcritical cases with the original injector (see Fig. 14), the dark core seems to be the shortest when the pressure perturbations are a minimum. Also, within the limits imposed by the calculated uncertainty, a significant reduction of the dark core length with respect to its non-forced value is observed during acoustic excitation at moderate J values. This decrease in the length, and therefore enhancement of mixing, is achieved in the $1 < J < 5$ range. At higher outer to inner jet momentum flux values the outer jet starts to entrain a significant amount of fluid from the inner jet inhibiting the effects of the acoustic field on the dark core.

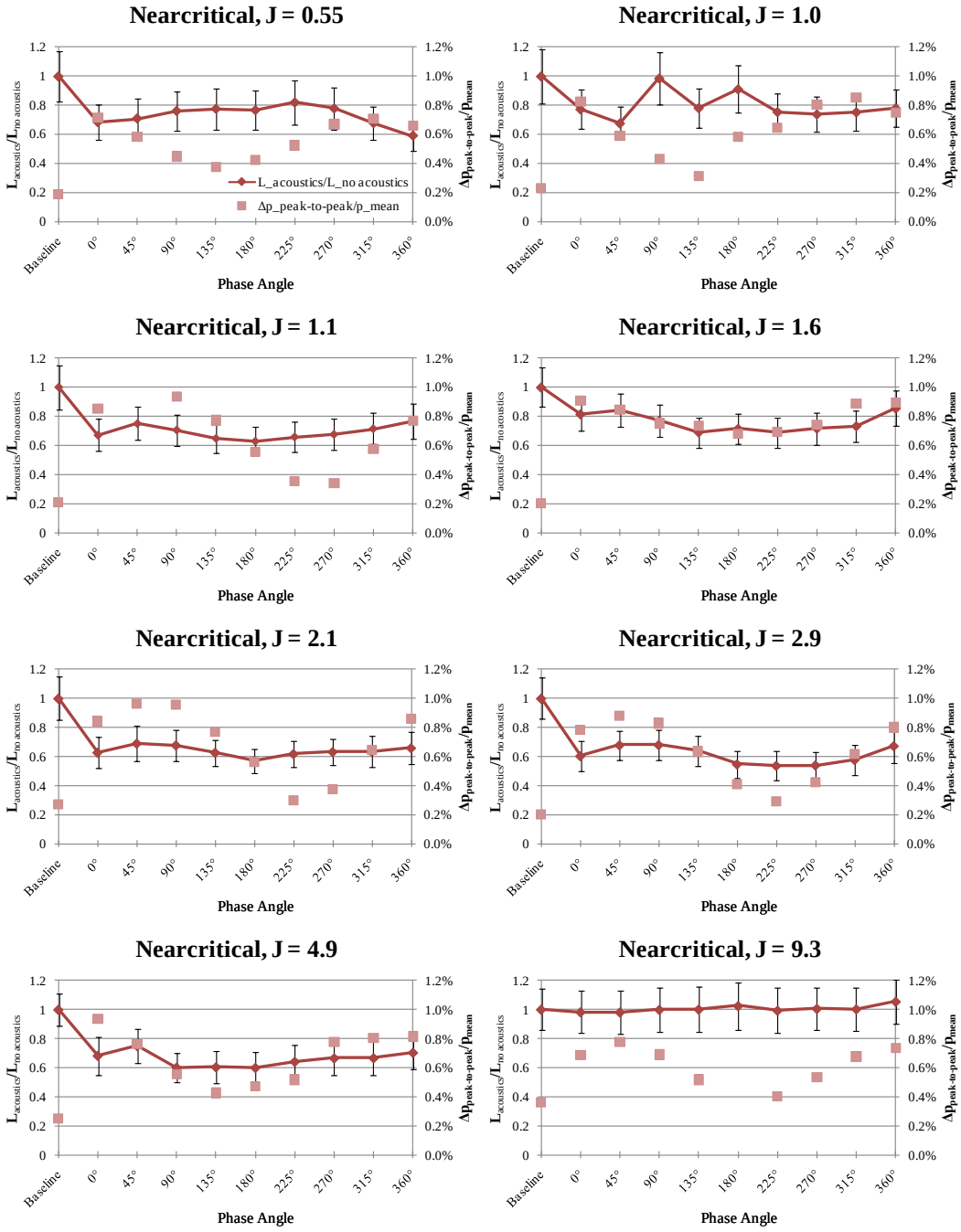

Figure 14. Dark core length with acoustics ($L_{acoustics}$) over dark core length without acoustics ($L_{no\ acoustics}$), shown in diamonds, versus phase angle between acoustic sources for nearcritical pressures. The the peak-to-peak pressure perturbation as a percentage of the mean chamber pressure ($\Delta p_{peak\text{-}to\text{-}peak}/p_{mean}$), in squares, is also plotted. Original injector geometry.

The set of plots in Fig. 15 presents the values of the dark core lengths for the tests at supercritical pressures with the original injector. These results also represent single-phase coaxial jet flow since the chamber, the inner jet, and the outer jet are at supercritical temperature and pressure conditions. In these cases, the amplitude of acoustic forcing does not go over 0.75% of the mean chamber pressure. From the supercritical pressure tests, within the limits of the uncertainty, a reduction of the dark core length similar to that observed for the nearcritical cases was accomplished. Again, the largest effects on length decrease and mixing enhancement were achieved in the $1 < J < 3$ range. For higher values, the inner jet starts to lose its core in a very rapid fashion to the outer jet which makes very difficult to distinguish the effects of the acoustic field on the dark core. Overall, it was difficult to see a trend between the location of the pressure node and the maximum length of the dark core.

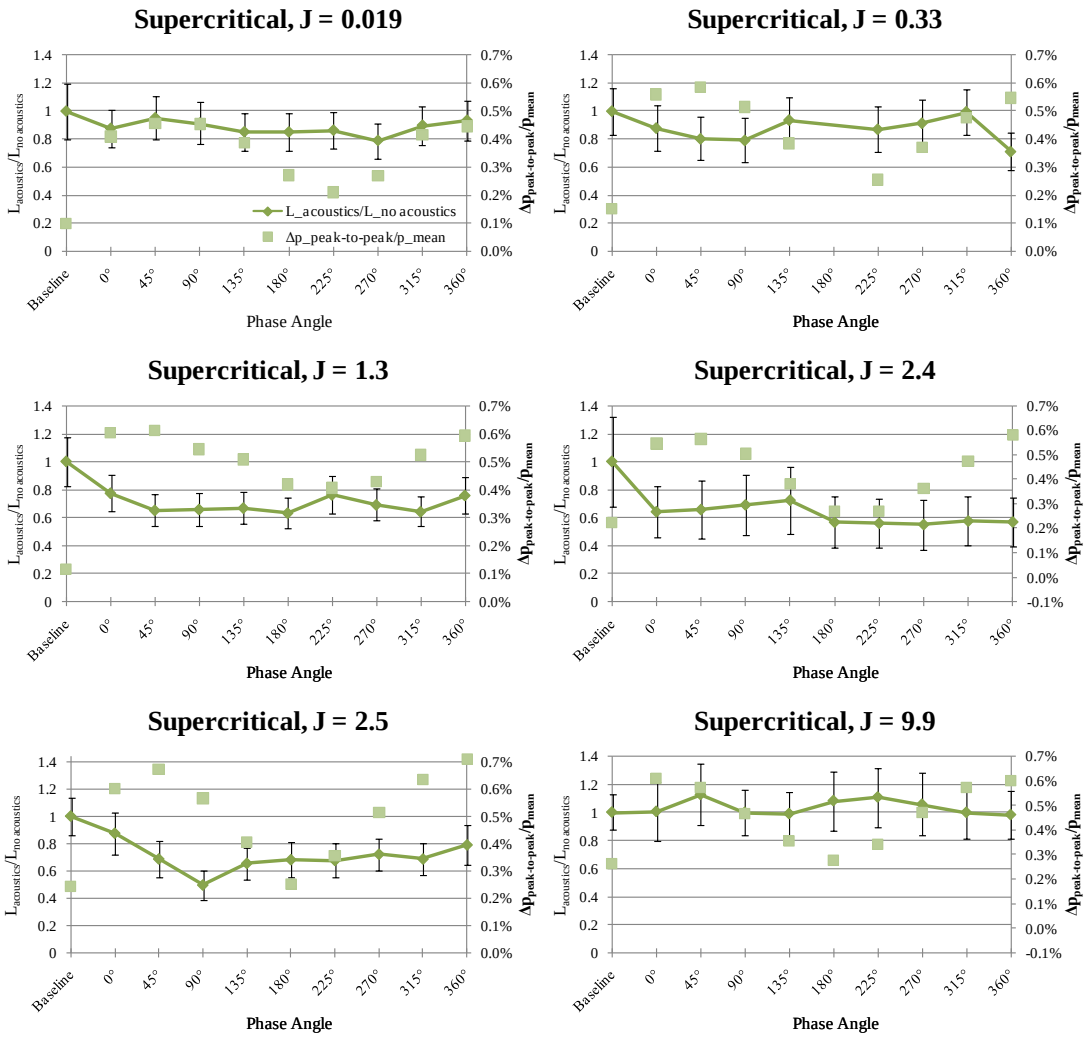

Figure 15. Dark core length with acoustics ($L_{acoustics}$) over dark core length without acoustics ($L_{no\ acoustics}$), shown in diamonds, versus phase angle between acoustic sources for supercritical pressures. The the peak-to-peak pressure perturbation as a percentage of the mean chamber pressure ($\Delta p_{peak\text{-}to\text{-}peak}/p_{mean}$), in squares, is also plotted. Original injector geometry.

The following set of plots in Fig. 16 show the behavior of the dark core length for the cases obtained when the pressure was above the critical point with the new injector. All conditions for the lower four momentum flux ratio cases showed dark cores that were longer than the field of view, explaining the results. Pressure profiles show that the coaxial jet was exposed to maxima and minima in pressure perturbations ranging from 0.2% to 1% of the mean chamber pressure; however, no effect on the dark core was seen. There were some instances, as in the 315° condition for the nearcritical case with J = 0.50 where the acoustic excitation modified significantly the mechanics

of the jet. Dark core lengths are not reported for such cases because the jet behavior departed signifincantly from the rest of the conditions. This behavior was observed at various J values near the pressure antinode condition at sufficiently high acoustic amplitudes. The nature of this phenomena is believed to be due to the lack of recirculation zone near the injector exit allowing high pressure fluctuations to interact with the inner jet leading to a violent disintegration of the dark core.

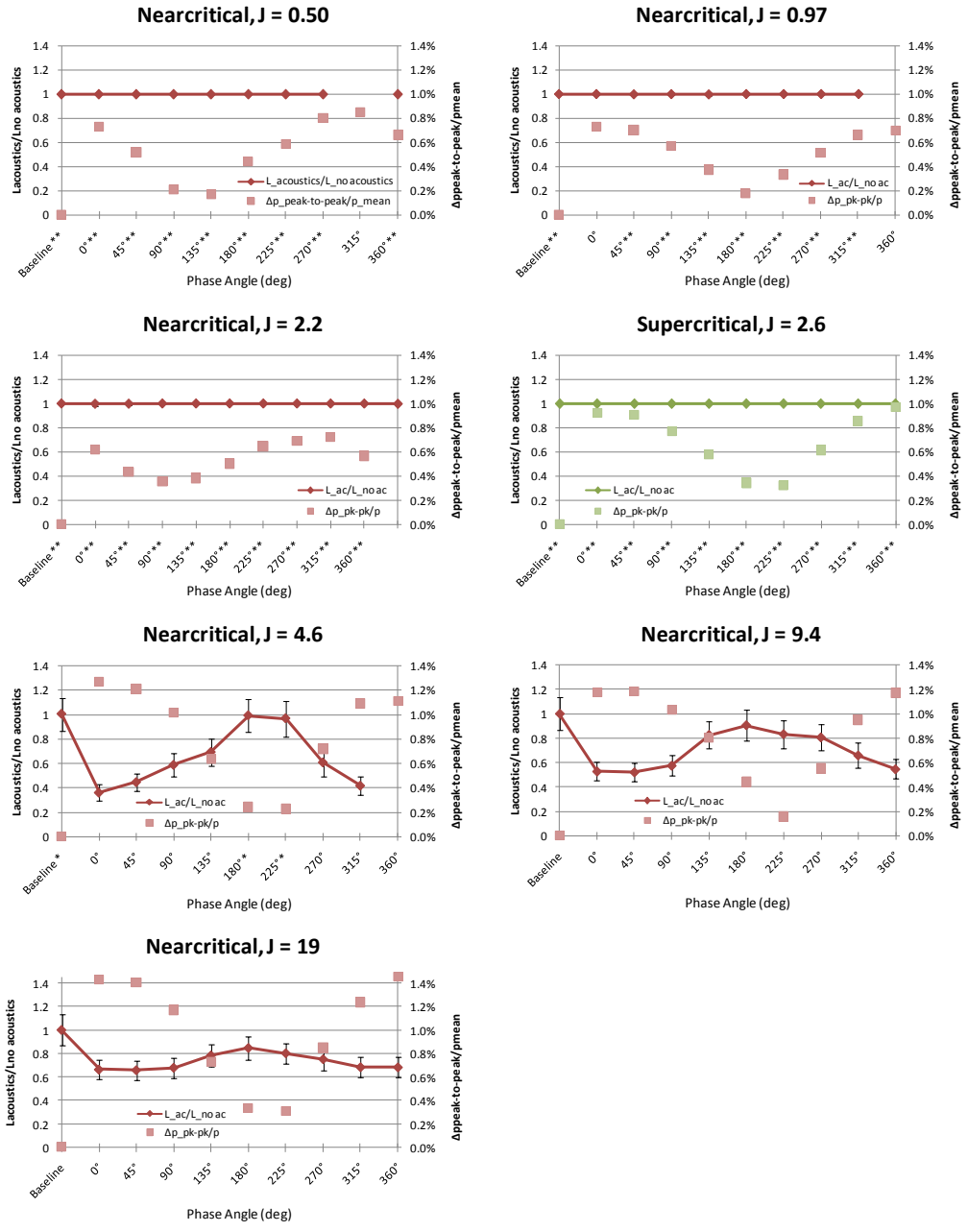

Figure 16. Dark core length with acoustics ($L_{acoustics}$) over dark core length without acoustics ($L_{no\ acoustics}$), shown in diamonds, versus phase angle between acoustic sources for pressures above the critical point. The the peak-to-peak pressure perturbation as a percentage of the mean chamber pressure ($\Delta p_{peak\text{-}to\text{-}peak}/p_{mean}$), in squares, is also plotted. See caption of Fig. 13 for further details. New injector geometry.

The results of the last three nearcritical cases in Fig. 16, however, show very interesting trends that match those of the subcritical results of the new injector in Fig. 13. For instance, the nearcritical case with J = 4.6 shows that, as the pressure node condition is approached, the dark core increases its length, reaching a maximum near a 180° phase angle. This behavior was also observed for the subcritical cases with momentum flux ratios of 3.4 and 5.2 (see Fig. 13). For the nearcritical case at J = 9.4 the dark core length reached a maximum near the pressure node. Finally, the nearcritical case at J = 19 had its maximum dark core length with acoustics at a phase angle of 180°, very close to the pressure node indicated by the pressure measurments.

The dark core length changes at different pressures for a given outer to inner jet momentum flux ratio are presented next. The ratio of the length of the dark core with acoustics to the length of the dark core with no acoustics ($L_{acoustics}/L_{no\ acoustics}$) and the peak-to-peak pressure perturbation as a percentage of the mean chamber pressure ($\Delta p_{peak\text{-}to\text{-}peak}/p_{mean}$) both as a function of the phase angle between acoustic sources are shown in Figs. 17 and 18.

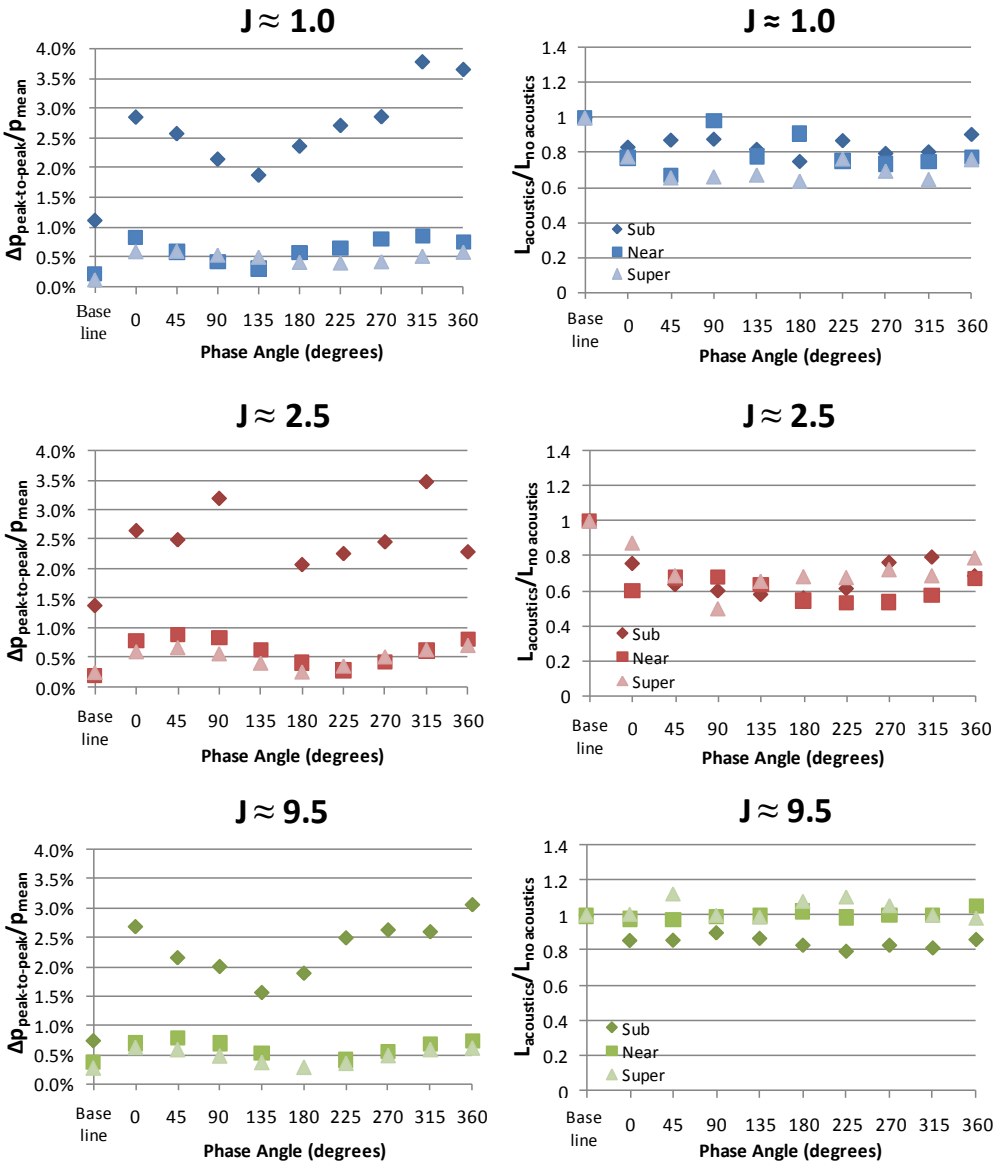

Figure 17. Peak-to-peak pressure perturbation ($\Delta p_{peak\text{-}to\text{-}peak}$) as a percentage of the mean chamber pressure (p_{mean}) and dark core length with acoustics ($L_{acoustics}$) over dark core length without acoustics ($L_{no\ acoustics}$) versus phase angle between acoustic sources for sub, near and superitical pressures at J ≈ 1.0, 2.5 and 9.5 for the original injector geometry. From Rodriguez et al.[11]

In Fig. 17 we observe the results for the original injector. Despite the relative acoustic excitation intensities varying several times from supercritical to subcritical conditions, the reduction in normalized dark core length (1 - $L_{acoustics}/L_{no\ acoustics}$) at most phase angles for J ≈ 1.0 ranged from 20% to 40%. When the outer to inner jet momentum flux ratio approaches 2.5 a similar trend is observed. The normalized dark core length now has a broader range reaching values as low as 50% of the baseline length and as high as 90% of the baseline length. The large spread could be a consequence of the inherent uncertainty of the measurements but still shows that acoustic forcing produces a clear shortening effect on the dark core length for J values near 2 to 3 as well. For outer to inner jet momentum flux ratios near 10, the largest reduction in the dark core length (1 - $L_{acoustics}/L_{no\ acoustics}$) is at most 20%, at subcritical pressures. Both nearcritical and supercritical cases show little or no reduction in their dark core length, in fact some of the data indicates that the dark core lengths actually increased in some cases. However, this phenomenon is the consequence of very small dark core lengths at these high J values.

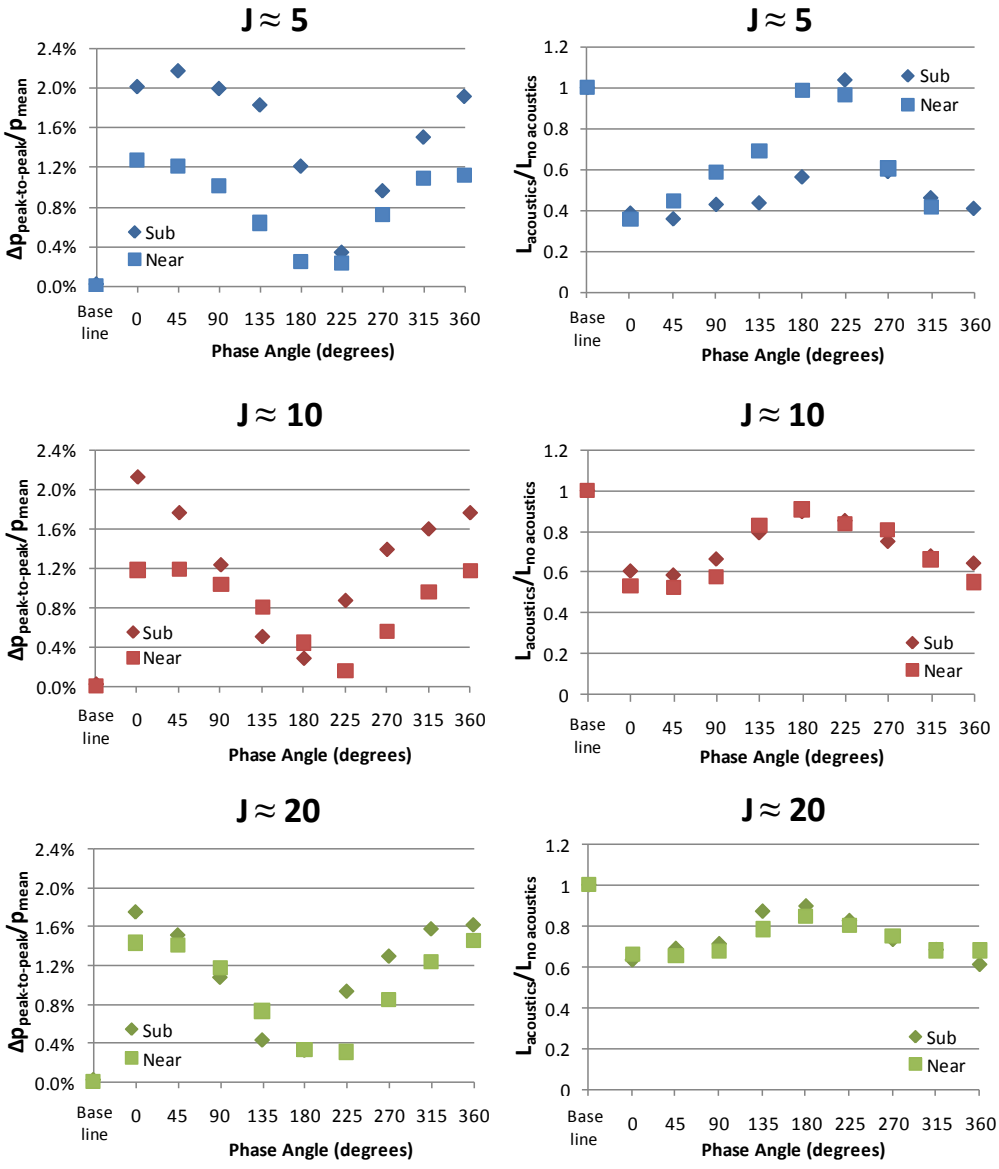

Figure 18. Peak-to-peak pressure perturbation ($\Delta p_{peak\text{-}to\text{-}peak}$) as a percentage of the mean chamber pressure (p_{mean}) and dark core length with acoustics ($L_{acoustics}$) over dark core length without acoustics ($L_{no\ acoustics}$) versus phase angle between acoustic sources for sub, near and superitical pressures at J ≈ 5, 10 and 20 for the new injector geometry. From Rodriguez[12].

Also at these conditions and especially true for near and supercritical conditions, the dark core does not show any response to acoustic forcing since most of the flow has been entrained by the outer jet and thus mixed with the rest of the fluid in the chamber, leaving a short dark core that usually does not show interesting acoustic behavior. Overall, these results with the original injector geometry show a very interesting trend which suggests that normalized dark core length behavior could be independent of mean chamber pressure; however, the large uncertainties in the measurements still prevent us from a definitve conclusion in this regard.

The same results for the new injector are shown in Fig. 18 above. A remarkable feature of these plots is the agreement in the relative dark core lengths between subcritical and nearcritical cases. As previously explained, data for lower J values are not available since the dark core length was longer than the acquired image. For a J value close to 5, the maximum pressure oscillations normalized by the mean chamber pressure are almost twice as much for the subcritical case compared to that of the nearcritical case. In contrast, for J near 20, the relative acoustic forcing is almost the same. Nonetheless, for each momentum flux ratio, the maxima and minima in normalized dark core length between subcritical and nearcritical pressures are very similar, regardless of the relative pressure oscillation. Therefore, the relative effect of the acoustics on the dark core length with the new injector for similar momentum flux ratios agrees with the results obtained with the original injector (see Fig. 17). Given the differences between the inner jet characteristics of the original and the new injector (inner post thickness, inner jet diameter, inner jet velocity and temperature), the agreement in dark core length results for the same J values indicates that this parameter could in fact reduce the data for a given geometry regardless of its characteristics. Further evidence of this observation could have important repercusions in shear coaxial injector design.

IV. Conclusions

In this study a new coaxial injector design was tested at three different pressure regimes and compared to the results obtained with a previously used injector. The new injector featured a larger cross-sectional area for the inner jet and a thinner wall between the inner and outer jet flows, resulting in a significantly smaller recirculation zone at the location where the inner and outer jets meet near the exit of the injector. There was a qualitative enhancement in mixing and atomization of the inner jet dark core with the surrounding outer jet and the chamber fluid obtained with this new injector.

The data obtained with the new injector extended the range at which acoustics had a noticeable effect on the coaxial flow to momentum flux ratios as low as 0.1 in the subcritical pressure regime when compared to the original injector. Testing at nearcritical and supercritical pressures showed a measureable response for J equal to 5 or greater. The quantitative analysis of the data for the new injector showed that the longest dark cores with acoustic excitation were observed at or near the pressure node location both at subcritical and supercritical conditions. The new injector thus provided evidence that different geometries for coaxial injectors of similar size could have an impact on the dynamics of a coaxial jet.

The fact that the results for the new injector show that the normalized dark core lengths ($L_{acoustics}/L_{no\ acoustics}$) for the different phase angle conditions at sub, near and supercritical cases agree remarkably well for a given outer to inner jet momentum flux ratio is evidence of similarity between the dynamics of the original and new injector. Both injectors showed the same large effect on the dark core at moderate J values and as the momentum flux ratio is increased the maximum reduction decreases. The comparison between the two geometries showed that acoustics can promote mixing enchancement through different mechanisms.

The results in this study showed that the relative acoustic pressure did not seem to severely affect the behavior of the dark core length for different pressures at the same outer to inner momentum flux ratio. This finding supports the possibility that only a small perturbation, equal or smaller than the relative amplitudes used in this study, is needed to achieve the same large reductions of the dark core length, and thus mixing enhancement, obtained with the largest perturbations. If the previous proposition is true, even small pressure perturbations could have a large impact on the stability behavior of LRE injectors and other applications of coaxial flows.

Appendix

A. Case Details for the Original Injector Tests

	$T_{chamber}$ (K)	$\rho_{chamber}$ (kg/m^3)	$P_{chamber}$ (MPa)	T_{outer} (K)	$\dot{m}_{outer}$ (mg/s)	ρ_{outer} (kg/m^3)	u_{outer} (m/s)	Re_{outer} (10^4)	T_{inner} (K)	$\dot{m}_{inner}$ (mg/s)	ρ_{inner} (kg/m^3)	u_{inner} (m/s)	Re_{inner} (10^4)	L/D_1 (baseline)	Freq. (kHz)	$P'_{RMS\ max}$ (kPa)	VR	J
SUB																		
sub1	233	22.0	1.50	191	310	27.6	4.30	0.768	109	279	630	2.2	1.2	26.2	2.98	21.5	2.0	0.17
sub2	231	22.2	1.50	183	790	28.8	11.0	2.02	109	283	630	2.2	1.2	17.1	3.06	20.1	4.8	1.0
sub3	226	21.9	1.45	183	1230	27.8	16.9	3.16	109	284	630	2.2	1.2	16.6	3.06	17.8	7.6	2.6
sub4	226	22.9	1.51	185	1560	28.7	20.9	3.96	109	279	630	2.2	1.2	15.2	2.96	15.7	9.5	4.2
sub5	210	24.9	1.50	182	2400	29.3	31.3	6.18	109	279	630	2.2	1.2	8.40	3.01	16.9	14	9.6
sub6	216	24.1	1.50	191	3640	27.7	50.3	9.02	109	279	630	2.2	1.2	5.63	3.02	16.3	23	23
NEAR																		
near1	223	56.6	3.58	180	1060	75.4	5.38	2.58	123	290	520	2.8	2.0	24.4	3.08	9.04	2.0	0.55
near2	207	62.0	3.57	152	1570	101	5.95	4.16	117	289	590	2.4	1.5	15.5	3.04	10.8	2.5	1.0
near3	228	55.1	3.58	185	1590	72.4	8.40	3.80	126	293	440	3.3	2.5	14.6	3.00	11.8	2.6	1.1
near4	223	56.1	3.55	184	2170	72.3	11.5	5.21	127	294	360	4.0	3.4	12.1	3.01	11.4	2.8	1.6
near5	230	54.2	3.56	199	2120	65.1	12.5	4.84	126	292	440	3.3	2.5	12.9	3.03	12.1	3.8	2.1
near6	229	54.5	3.56	183	2690	73.1	14.1	6.48	126	292	420	3.4	2.5	5.98	3.05	11.1	4.1	2.9
near7	219	57.6	3.56	194	3080	67.4	17.5	7.15	125	289	480	3.0	2.2	5.56	3.06	11.8	5.9	4.9
near8	213	59.6	3.56	192	6460	68.3	36.2	15.1	128	295	220	6.6	5.2	2.45	2.93	9.73	5.5	9.3
SUPER																		
super1	231	76.1	4.96	198	292	93.9	1.19	0.642	136	291	300	4.8	3.9	37.7	3.05	8.01	0.25	0.019
super2	231	76.1	4.96	193	997	97.7	3.90	2.22	130	292	460	3.1	2.4	26.7	3.01	10.2	1.2	0.33
super3	221	80.4	4.95	180	2050	109	7.19	4.72	128	291	490	2.9	2.1	19.2	3.01	10.7	2.5	1.3
super4	222	80.1	4.96	182	3110	107	11.1	7.13	134	288	360	3.9	3.3	10.2	3.05	10.1	2.8	2.4
super5	222	80.3	4.97	191	2820	99.5	10.8	6.32	131	293	440	3.3	2.6	9.02	3.09	12.5	3.3	2.5
super6	211	85.8	4.96	187	5820	103	21.6	13.2	132	286	410	3.4	2.7	3.04	3.05	10.7	6.3	9.9

B. Case Details for the New Injector Tests

	$T_{chamber}$ (K)	$\rho_{chamber}$ (kg/m^3)	$P_{chamber}$ (MPa)	T_{outer} (K)	$\dot{m}_{outer}$ (mg/s)	ρ_{outer} (kg/m^3)	u_{outer} (m/s)	Re_{outer} (10^4)	T_{inner} (K)	$\dot{m}_{inner}$ (mg/s)	ρ_{inner} (kg/m^3)	u_{inner} (m/s)	Re_{inner} (10^4)	L/D_1 (baseline)	Freq. (kHz)	$P'_{RMS\ max}$ (kPa)	VR	J
SUB																		
subnew1	235	22	1.48	199	90	26	1.4	0.21	105	920	660	0.91	1.3	13+	3.01	8.86	1.5	0.089
subnew2	237	22	1.49	197	200	26	3.0	0.47	106	925	655	0.92	1.3	13+	2.96	14.0	3.3	0.43
subnew3	246	21	1.49	195	450	27	6.6	1.1	109	925	630	0.96	1.5	11+	2.97	12.1	6.9	2.0
subnew4	224	23	1.49	189	600	28	8.5	1.5	110	925	620	0.97	1.5	10.4	3.04	10.2	8.7	3.4
subnew5	217	24	1.49	184	750	29	10	1.9	110	925	620	0.97	1.5	9.29	3.02	11.5	11	5.2
subnew6	228	22	1.49	193	880	27	13	2.1	108	925	640	0.94	1.4	8.08	2.96	12.7	14	7.8
subnew7	222	23	1.49	194	1100	27	16	2.6	108	925	640	0.94	1.4	7.63	2.92	11.2	17	12
subnew8	217	24	1.48	201	1300	26	20	3.0	109	925	630	0.96	1.5	7.26	2.90	9.16	21	18
NEAR																		
nearnew1	228	55	3.56	213	330	60	2.2	0.70	109	925	650	0.93	1.3	14+	2.98	10.8	2.3	0.50
nearnew2	226	55	3.56	209	460	61	3.0	1.0	109	925	650	0.93	1.3	14+	3.06	9.17	3.2	0.97
nearnew3	230	54	3.58	198	730	66	4.3	1.6	108	925	655	0.92	1.3	13+	3.00	9.12	4.7	2.2
nearnew4	216	59	3.58	199	1030	65	6.3	2.3	109	925	650	0.93	1.3	13+	3.11	16.0	6.7	4.6
nearnew5	214	59	3.58	203	1460	63	9.2	3.2	109	925	650	0.93	1.3	7.01	3.07	15.0	9.9	9.4
nearnew6	215	59	3.56	207	2060	62	13	4.5	111	925	635	0.95	1.4	3.55	3.09	18.3	14	19
SUPER																		
supernew1	219	81	4.95	212	890	85	4.1	1.8	111	925	650	0.93	1.4	13+	3.11	17.0	4.4	2.6

Acknowledgements

The authors would like to express their appreciation to Mr. Randy Harvey for his invaluable contributions in running and maintaining the facility. This work is sponsored by AFOSR under Mitat Birkan, program manager.

References

1. Gutmark, E., Schadow, K. C., Wilson, K. J., "Mixing Enhancement in Coaxial Supersonic Jets*", AIAA-89-1812*.
2. Gautam, V., Gupta, A. K., "Simulation of Flow and Mixing from a Cryogenic Rocket Injector", *Journal of Propulsion and Power*, Vol. 23, No. 1, 2007, pp. 123-130.
3. Zong, N., Yang, V., "A Numerical Study of High-Pressure Oxygen/Methane Mixing and Combustion of a Shear Coaxial Injector", *AIAA-2005-0152*.
4. Richecoeur, F., Scouflaire, P., Ducruix, S., Candel, S., "High-Frequency Transverse Acoustic Coupling in a Multiple-Injector Cryogenic Combustor", *Journal of Propulsion and Power*, Vol. 22, No. 4, 2006, pp. 790-799.
5. Leyva, I. A., Chehroudi, B., Talley, D., "Dark-Core Analysis of Coaxial Injectors at Sub-, Near-, and Supercritical Conditions in a Transverse Acoustic Field", *54th JANNAF Meeting*, Denver, CO, May 14-18, 2007.
6. Leyva, I. A., Chehroudi, B., Talley, D., "Dark-Core Analysis of Coaxial Injectors at Sub-, Near-, and Supercritical Conditions in a Transverse Acoustic Field", *AIAA-2007-5456*.
7. REFPROP, Reference Fluid Thermodynamic and Transport Properties, Software Application Ver. 7.0, NIST, Gaithersburg, MD, U. S. Department of Commerce, 2002.
8. Thermophysical Properties of Fluid Systems, Online Database, NIST, U. S. Department of Commerce, 2005. http://webbook.nist.gov/chemistry/fluid.
9. Otsu, N., "A Threshold Selection Method from Gray-Level Histograms", IEEE Transactions on Systems, Man and Cybernetics, Vol. 9, pp. 62-66.
10. Davis, D. W., "On the Behavior of a Shear-Coaxial Jet, Spanning Sub- to Supercritical Pressures, with and without an Externally Imposed Transverse Acoustic Field", Ph. D. Dissertation, Department of Mechanical and Nuclear Engineering, Pennsylvania State University, 2006.
11. Rodriguez, J. I., Leyva, I. A., Chehroudi. B., Talley, D., "Results on Subcritical One-Phase Coaxial Jet Spread Angles and Subcritical to Supercritical Acoustically-Forced Coaxial Jet Dark Core Lengths", 44th AIAA/ASME/SAE/ASEE Joint Propulsion Conference and Exhibit, Hartford, CT, 21-23 July 2008.
12. Rodriguez, J. I., "Acoustic Excitation of Liquid Fuel Droplets and Coaxial Jets", Ph. D. Dissertation, Department of Mechanical and Aerospace Engineering, UCLA, 2009.